

Documentation - Theory

# Interferometric SAR Processing



Version 1.0 – November 2007

**GAMMA Remote Sensing AG**, Worbstrasse 225, CH-3073 Gümligen, Switzerland  
tel: +41-31-951 70 05, fax: +41-31-951 70 08, email: [gamma@gamma-rs.ch](mailto:gamma@gamma-rs.ch)

## Table of contents

1.	INTRODUCTION .....	4
2.	PRE-PROCESSING .....	5
2.1.	<i>Data transcription and modification</i> .....	5
2.2.	<i>Manipulation of orbital state vectors</i> .....	6
2.2.1.	DELFT orbits.....	6
2.2.2.	PRC Precision Orbits.....	6
2.2.3.	DORIS precision orbits.....	7
2.3.	<i>Calibration</i> .....	7
3.	CO-REGISTRATION.....	8
4.	BASELINE ESTIMATION .....	9
5.	COMMON BAND FILTERING AND INTERFEROGRAM CALCULATION .....	11
6.	INTERFEROGRAM FLATTENING .....	12
7.	COHERENCE ESTIMATION .....	13
8.	INTERFEROGRAM FILTERING.....	14
9.	PHASE UNWRAPPING.....	15
10.	PRECISE BASELINE ESTIMATION .....	17
11.	COMPUTATION OF HEIGHTS / RESAMPLING TO MAP COORDINATES.....	17
12.	DIFFERENTIAL INTERFEROMETRIC PROCESSING .....	19
12.1.	<i>Generation of differential interferogram / removal of topographic phase</i> .....	19
12.1.1.	2-pass differential interferometry .....	20
12.1.2.	3-pass differential interferometry .....	21
12.1.3.	4- pass differential interferometry .....	23
12.1.4.	Combination of interferograms .....	24
12.2.	<i>Extraction of topographic phase / removal of differential phase</i> .....	25
	REFERENCES .....	27
	ADDITIONAL BIBLIOGRAPHY ON SAR INTERFEROMETRIC PROCESSING .....	28

## List of acronyms

ALOS	Advanced Land Observing Satellite
ASAR	Advanced Synthetic Aperture Radar
DEM	Digital Elevation Model
DEOS	Department Earth Observation and Space Systems
ENVISAT	ENVIronmental SATellite
ERS	European Remote Sensing (Satellite)
ESA	European Space Agency
ESRIN	European Space Research Institute
FFT	Fast Fourier Transform
GCP	Ground Control Point
GFZ	GeoForschungsZentrum Potsdam
InSAR	SAR interferometry
ISP	Interferometric SAR Processor
JERS	Japanese Earth Resources Satellite
MCF	Minimum Cost Flow
PAF	Product Archiving Facility
PALSAR	Phased Array L-band Synthetic Aperture Radar
SAR	Synthetic Aperture Radar
SLC	Single Look Complex
SRTM	Shuttle Radar Topography Mission
TCN	Track, Cross-track, Normal
TIN	Triangular Irregular Network
USGS	United States Geological Survey
WGS	World Geodetic System

## **1. Introduction**

The expression “interferometric SAR processing” refers to the generation of an interferogram starting from a pair of images in Single Look Complex format (SLC). Starting from the two complex SAR images, interferometric processing consists of a number of steps (see below) that allow the estimation of the interferometric phase and the coherence.

- Co-registration of the two complex images
- Common-band filtering in range and azimuth
- Generation of the interferogram
- Estimation of the interferometric baseline
- Removal of curved Earth phase (i.e. phase flattening)
- Estimation of the interferometric coherence
- Filtering of an interferogram
- Phase unwrapping

In addition, SAR interferometric processing includes the conversion of the interferometric phase to obtain a measure of elevation and orthorectification of interferometric images and products, i.e. transformation from slant range to ground range coordinates. Finally, even though it is not directly related to interferometric processing, calibration of the SAR images forming an interferometric pair allows further use of the intensity images.

These steps can be considered as forming the standard interferometric processing sequence; however, the sequence should not be considered as fixed. Depending on the interferometric products to be obtained and on the quality of the products (i.e. precision of the estimates), some steps can be repeated at various stages throughout the processing. For example the estimation of the baseline is required twice if the interferometric phase is to be used for generation of an elevation map. A first rather precise estimate is required when flattening the interferogram; a more precise estimate is necessary in case the phase is unwrapped.

Interferometric processing and differential interferometric processing are strongly interlinked in the sense that several steps of the interferometric processing are applied when generating differential interferograms (e.g. refinement of the baseline, interferogram filtering, phase unwrapping) and differential interferograms can be used in interferometric processing (e.g. to estimate the coherence).

The flowchart in Figure 1 shows schematically the interferometric SAR processing phases. Input and output data are also illustrated. The flowchart can be considered general although it is referred to the processing sequence in the Interferometric SAR Processor (ISP) package of the GAMMA software.

Before proceeding to processing, a set of pre-processing steps can be applied. The SLCs must be transcribed from support media and put in a format that is understood by the interferometric processor. If necessary (and possible), the orbit state vectors should be improved. Radiometric calibration of intensity images can be performed. All these aspects will be treated in Section 2. Section 3 to Section 12 described each step of the interferometric processing individually. A list of relevant publications on interferometric SAR processing is provided at the end of this document.

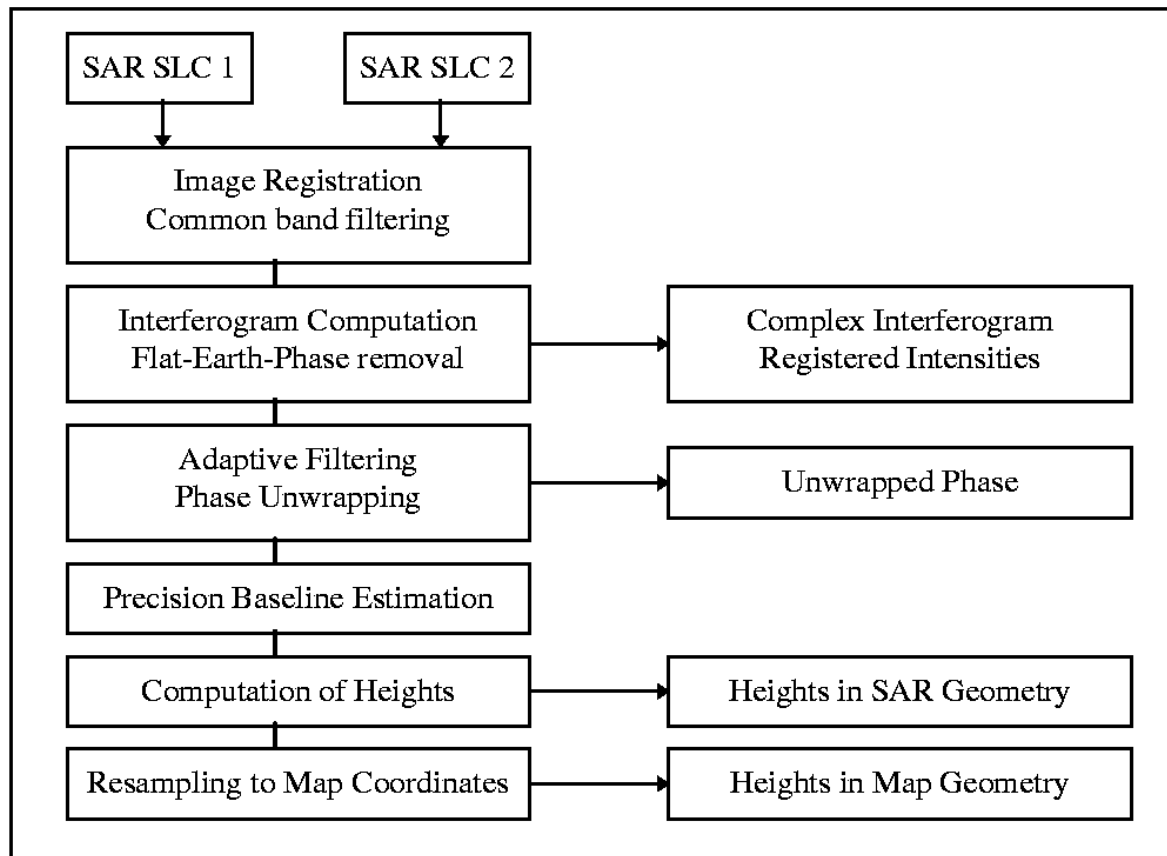


Figure 1. Standard interferometric processing chain

## 2. Pre-processing

### 2.1. Data transcription and modification

While the term “SLC” indicates that each pixel corresponds to a single look and is a complex number, SLC images can have different formats:

- the number of bytes for real and the imaginary part can be 2 or 4, resulting in pixels of 4 or 8 byte. In the first case one refers to SLC in short complex format, in the second case to SLC in float complex format.
- the image data file might purely contain the complex values or include a header including metadata describing the image properties. The header can be at the beginning (e.g. for ENVISAT ASAR data) or on each line (e.g. ALOS PALSAR SLC). For TerraSAR-X data are provided in an archive file consisting of a selection of annotation and data files.

The format of an SLC depends on the SAR processor used, i.e. the facility distributing the SLC data. Even for a given SAR sensor the format of the SLC can be different depending on the entity distributing the data. Hence, it is important to know the format of the image data (and the metadata accompanying the image data) to proceed without problems in interferometric processing. After transcription of the data from support media to the computer, modification of the SLC to adapt it to the interferometric processor used is necessary in most cases. Modification also includes taking a subset of an SLC. Subsetting is

recommended in case the user is interested in a small part of the image only. In this way the processing speed is significantly increased.

## **2.2. Manipulation of orbital state vectors**

State vectors are typically provided with the image data by the data processing facilities and include instant position and velocity of the satellite components expressed in the Earth-centered Cartesian coordinate system. In some cases the number of state vectors provided with the image data might be insufficient for correct processing or cover an area that is too small compared to the length of the image to be processed. For this reason additional state vectors need to be introduced by respectively interpolation of the available state vectors and orbit propagation.

Another problem, which basically concerns all spaceborne SAR systems except the most recent (e.g. ALOS PALSAR and TerraSAR-X), is that the orbit data provided with the image data file is not precise enough. This is a drawback for example when flattening the interferogram or doing phase unwrapping (see Section 10). Precise orbit for ERS and ENVISAT can be obtained from several sources listed below. No precise orbit data is available for JERS-1 and RADARSAT-1. Precise orbits are introduced in the metadata describing the SLC substituting the original state vector information.

### **2.2.1. DELFT orbits**

The Department of Earth Observation and Space Systems (DEOS) at the Technical University of Delft provides highly precise orbits for ERS-1, ERS-2 and ENVISAT, in support of altimetric and interferometric SAR research. The DELFT orbit data (and the software that supports their manipulation) can be obtained from the DEOS website <http://www.deos.tudelft.nl/ers/precorbs>. The orbits are distributed as files (\*.ODR) for ERS-1, ERS-2, and ENVISAT. The ODR data sets have significant overlap and cover approximately 3 to 5 days of orbital data. The list of ODR files available at DEOS including the start and end date for each ODR file is available in the text file *arclist*. Details on the DELFT package and state vector format are available at the DEOS website.

### **2.2.2. PRC Precision Orbits**

PRC orbits are made available for ERS-1 and ERS-2 by ESA. The precise orbit results from a data reduction process in which all available tracking data and most accurate correction, transformation and dynamical models are taken into account and in which high level numerical procedures are applied. Processing is carried out by D-PAF and GFZ Potsdam. More information is available at the dedicated website <http://earth.esa.int/services/pg/pgersorbprc.xml>.

The PRC data are available from an ftp server in Germany with a delay of about 1 month after data acquisition by ERS. Apply to the ESA Helpdesk at ESA ESRIN to get an account to access these data (eohelp@esa.int). The PRC data contain the position and velocity of the sensor in both body-fixed and inertial coordinates. Sensor attitude data is also kept with the state vectors. PRC data are available with a delay of about 1 month and cover a period of about 5-7 days each. The PRC filenames contain the date of the first state vector and the starting orbit number.

The PRC files consist of 130 byte text records containing the Julian date and time of the state vector data, the position, velocity and attitude of the ERS sensor, and data quality information. State vectors are given on 30 second intervals. The format of the PRC data file records is described in an ESA document available from the abovementioned ESA ESRIN website.

### 2.2.3. DORIS precision orbits

Precise orbits for ENVISAT are determined from Doppler shift data measured by the DORIS instrument. The precise orbit reconstruction is the most accurate orbit estimate produced from the DORIS data. The file is used during ground processing and is updated once per day.

A file containing DORIS precision orbits consists of 129 byte text records containing the date, time, offset between UTC and UT1, orbit, position, and velocity, and data quality information. State vectors are given on 60 second intervals.

The format of the DORIS data file records is described in an ESA document available from <http://envisat.esa.int/dataproducts/asar/CNTR2-9-3.htm>. Access to the DORIS data is via a request to the ESA ESRIN Helpdesk (eohelp@esa.int). Data are available on an ESA ftp site and are updated with 4-6 weeks delay from acquisition. The orbit data are arranged in files covering a full day and extending to the previous day by a couple of hours. Data are available starting July 22, 2002. For previous dates the DELFT orbits should be considered. The DORIS orbits file name starts with DOR\_VOR\_AXVF-. Then date and time of processing, start date and time of the orbit data, end date and time of the orbit data follow. Format for the date is `yyyymmdd`. Format for the time is `hhmmss` (e.g. `DOR_VOR_AXVF-P20020906_120800_20020722_215528_20020724_002328`).

## 2.3. Calibration

The magnitude of the SLC might not uniform all over the scene but suffer from different effects related e.g. to the pattern of the antenna diagram, the longer traveling path of a wave in far range compared to near range etc. To adjust the magnitude level of the image, relative calibration is needed. Relative calibration of an image takes into account the antenna pattern in range, the variation in slant range, and the variation in length of the azimuth reference function, the interpolation window function, the ground-surface projection for a horizontal surface. An additional factor needs to be then considered for absolute radiometric calibration.

A calibrated SLC can be either in the *sigma0* or in the *gamma0* form. In the *sigma0* case the SLC image intensity (SQR(re)+SQR(im)) corresponds to the backscattering coefficient  $\sigma^o$  (normalized to the horizontal ground surface). In the case of *gamma0* the SLC image intensity (SQR(re)+SQR(im)) corresponds to the backscattering coefficient  $\gamma^o$ , which is related to  $\sigma^o$  by

$$\gamma^o = \sigma^o / \cos \theta \quad (1)$$

with  $\theta$  being the incidence angle of the horizontal surface.

### 3. Co-registration

The SLCs forming an image pair do not overlap so that the computation of the interferogram requires first a co-registration step so that corresponding pixels in the two images perfectly match. Since all the information contained in the SLC to be resampled should be preserved, the accuracy in the co-registering operations must be exceptional, i.e. at sub-pixel level. Figure 2 shows that a registration accuracy of better than 0.2 pixels is required in order not to reduce the interferometric correlation by more than 5%. Precision co-registration requires using the image data to obtain residual errors  $< .05$  pixel

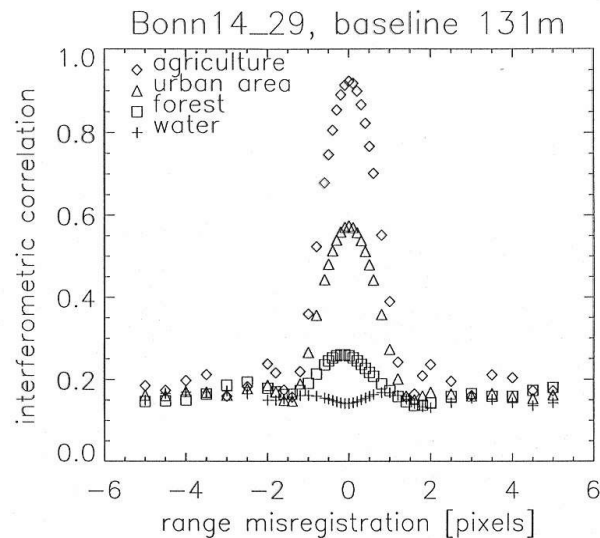


Figure 2. Interferometric correlation as function of varying misregistration in range between two SLCs (ERS-1, 1 pixel equals 20 m).

Co-registration typically consists of computation of offsets between the two SLCs and resampling one SLC in order to match with the reference image. The offsets are used to determine the coefficients of the interpolation function needed for the resampling.

The offsets between the SLC images can be computed using orbit data, correlation of image intensities or fringe visibility.

With the intensity cross-correlation optimization procedure, also known as intensity tracking, a number of windows distributed over the image is set and offset fields are generated with a normalized cross correlation of image patches of detected real-valued SAR intensity images. The successful estimation of the local image offsets depends on the presence of nearly identical features in the two SAR images at the scale of the employed patches. The location of the peak of the 2-D cross-correlation function yields the image offset.

With coherence tracking, also known as the fringe visibility algorithm or coherence optimization procedure, small data patches are selected throughout the SLCs. A series of small interferograms with changing offset is constructed and the coherence is estimated. The location of the coherence maximum determines the local offset. The magnitude of the coherence maximum relative to the average level is used as a quality factor to help reject unsuitable patches.

Offsets are then used as inputs to a Least Squares polynomial fit. The polynomial is a biquadratic function. Generally a simple polynomial model is sufficient for the offset function between SLCs. In the case of large scale topography and a large baseline, this is no longer sufficient. A smart procedure when generating the polynomial is to use an approach that rejects offsets far from initial fit.

The stringent requirement on the misregistration error is satisfied only when complex interpolation filters are used. Theoretically one should use an ideal interpolator with a flat spectrum, i.e. an infinite sinc function. This is not possible because filters only have a finite length; nevertheless, as most of the SAR products are oversampled, the use of finite filters will not cause a loss of information. Resampling of the slave SLC image is typically performed using a complex sinc interpolator. As a matter of fact, every band-limited signal can be reconstructed from discrete samples acquired at the Nyquist rate.

#### 4. Baseline estimation

Estimation of the baseline is required for a number of operations: common band filtering (Section 5), flattening of the interferogram (Section 7), phase unwrapping (Section 10) and derivation of interferometric heights from the unwrapped phase (Section 12).

The interferometric baseline is defined as the difference of platform position vectors (actually antenna phase centers on the two passes) when a given scatterer is imaged. If the tracks are not parallel (typical for repeat-pass interferometry) the baseline changes along-track.

The position on the track when the SAR images a point depends on the effective squint of the radar. Depending on the Doppler range dependence the effective platform positions will change as a function of range. Image deskew changes the SAR image geometry to appear in the zero-Doppler geometry independent of Doppler centroid used to process the data. The baseline is not changed by different processing algorithms

The baseline can be decomposed into components. A reference system is can be the local coordinate system called TCN (Track, Cross-track, and Normal) coordinates. These are defined (see also Figure 3):

$$\hat{n} = \frac{-\vec{P}}{|\vec{P}|} \quad \hat{c} = \frac{\hat{n} \times \vec{V}}{|\hat{n} \times \vec{V}|} \quad \hat{t} = \hat{c} \times \hat{n} \quad (2)$$

In (2)  $\hat{t}$  the unit vector along the local flight direction, i.e. the direction of the platform's velocity vector  $\vec{V}$ .  $\hat{n}$  represents the unit vector along the nadir direction, i.e. the direction of the platform's position vector with respect to the Earth center,  $\vec{P}$ . Finally,  $\hat{c}$  is the unit vector in the direction perpendicular to the plane identified by the position and velocity vectors. Typically the out of plane component  $\hat{t}$  is negligible so that we have 2 major components only (cross-track and normal). The parallel baseline is the component along the radar's line of sight, the perpendicular baseline is the component perpendicular to the line of sight. Transformation between the TCN and the parallel-perpendicular reference system is based on simple trigonometric functions.

The measurement of the distance between the two SAR antennas in space when they image the same object on the ground is rather hard because it requires perfect knowledge of the satellites position and attitude as they travel along their orbit. In practice the baseline is estimated using a model of the baseline, the complexity of which can vary depending on the approach used and the precision one wants to obtain.

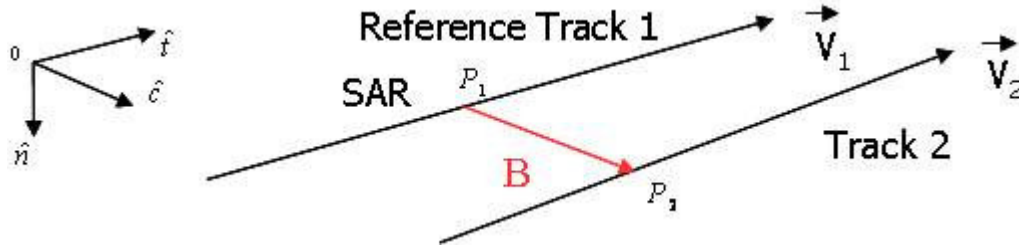


Figure 3. Representation of interferometric baseline estimation method using orbital state vectors

The baseline can be estimated using

- Orbital information
- Fringe rate of the interferogram (see also Section 7)
- Ground control points (after unwrapping, see also Section 11)

The method based on state vectors is illustrated in Figure 3. At first a point in the center of the scene is selected and the reference system basis is constructed, e.g. with axis along track, across track and normal (Track, Cross-track, Normal). The spacecraft location along the second track is then moved until the point of closest approach to the position of the spacecraft on the reference track is found. The vector between the spacecrafts is the baseline estimate.

It is clear that the method works fine when accurate state vectors are available. For ERS and ENVISAT updating the state vectors (see Section 2.2) has the effect of a rather accurate baseline estimation. For JERS-1 and RADARSAT-1 the state vectors are inaccurate and no correction is possible; therefore, this method is not reliable. PALSAR state vectors seem to be rather accurate, which implies that the baseline estimated with this method is rather accurate.

In the absence of reliable state vector information, the local fringe rate at the center of interferogram can be used to obtain an estimate of the perpendicular baseline. The local fringe rate in the unflattened interferogram can be calculated by taking:

$$\frac{\partial \phi}{\partial R} = -\frac{4\pi}{\lambda R \tan \theta} B_n \quad (3)$$

where  $\frac{\partial \phi}{\partial R}$  represents the fringe rate,  $\lambda$  the wavelength,  $R$  the slant range distance,  $\theta$  the local incidence angle and  $B_n$  the perpendicular component of the baseline. Over a small range of incidence angles, the fringe rate is constant so that this is easily detected when calculating an FFT of a region. Since the FFT gives the frequency of the fringes, Equation (3) can then be used to solve for the baseline.

An iterative flattening is possible by applying the algorithm multiple times, each time removing a residual fringe rate (see also Section 7 for flattening).

The method works fine when the fringes due to the curved Earth are the dominant interferometric phase component. For this reason regions should be chosen where topography is rather flat, atmospheric artifacts are limited, noise due to low correlation areas (forests, water etc) is negligible and no displacements between images acquisition have occurred.

The baseline estimation method based on ground control points (GCPs) is the most accurate. However, this can only be used for the inversion of the unwrapped phase to height (see Section 12) since elevation information of GCPs and interferometric phase directly related to an elevation information are required. This method is further described in Section 11.

## 5. Common band filtering and interferogram calculation

Let us first of all consider two platforms without squinting, i.e. the look directions of the two SARs are contained in the plane perpendicular to the flight direction. If the perpendicular baseline of the interferometric system is non-zero, i.e. two SAR view the scene under (slightly) different look angles, the band of the signal received by the one radar presents an offset with respect to the band of the signal received by the other radar. The consequence is that the two signals do not fully correlate, i.e. in other words the interference pattern between the images is somewhat corrupted. Total destruction of the interferometric fringes occurs when the spatial separation of the two SAR in space is such that the spectra do not overlap (i.e. critical baseline).

More in detail, the radar pulse samples a small bandwidth of the spatial reflectivity spectrum of the surface. This is illustrated in Figure 4 by the red bar “Spectrum 1”, which starts at  $k_{min}$ . Because the second interferometer antenna sees the scene from a slightly different look angle, it records a different part of the spectrum shifted by a certain amount  $\Delta f$ . This part is illustrated in Figure 4 by the blue bar “Spectrum 2”, which ends at  $k_{max}$ .

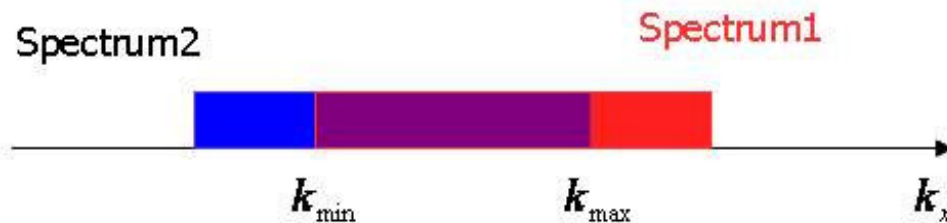


Figure 4. Illustration of spectral overlap of bands for two images acquired in a non-zero baseline interferometric system.

The frequency misalignment is given by

$$\Delta f = \frac{fB_n}{2R \tan(\theta - \xi)} \quad (4)$$

where  $\xi$  represents the local slope angle. Equation (4) shows that the effect increases for increasing perpendicular component of the baseline. This Equation can be used to determine the critical baseline, i.e. the baseline for which the interference between the two images is null or, in other words, complete decorrelation occurs.

When the slant range spectra of two images do not overlap completely, the non-common parts cause decorrelation and therefore must be filtered out prior to the generation of the interferogram. Spectral shift filtering removes the effect of baseline decorrelation for level surfaces. It consists of several operations and requires accurate baseline estimation (from orbital parameters) and slope estimation. For details see (Gatelli et al., 1994). The drawback is a proportional loss of range resolution because of the smaller bandwidth.

If the SAR antennas have different squint angles at acquisition, the two images have a slight difference in the azimuth spectra. The shift between the two spectra is due to a Doppler centroid not equal to zero frequency. This is the case of ERS-1/2 pairs for example. To remove this effect, azimuth bandpass filtering is generally performed to retain the parts of the band common to the two images. At first the Doppler centroid frequency is estimated and then the bandpass filter is applied to fit the Doppler centroid (Schwäbisch et al., 1995).

The complex interferogram is obtained from the cross-product of the co-registered SLCs and after common-band filtering. The interferogram consists of magnitude (correlation between images) and phase (InSAR phase). The correlation indicates how accurate the phase information is (fringe visibility). The lower the correlation, the noisier the phase. The InSAR phase is a combination of several contributions (curved Earth, topography, surface displacements, atmospheric delays and phase noise), which are schematically described in the Equation below:

$$\phi = \phi_{flatEarth} + \phi_{topography} + \phi_{displacement} + \phi_{delay} + \phi_{noise} \quad (5)$$

It should be noticed that the InSAR phase has values between 0 and  $2\pi$ , i.e. the phase is wrapped in this interval.

## 6. Interferogram flattening

The interferogram as generated from the SLCs has an almost linear phase trend across the image as a function of the slant range and baseline:

$$\frac{\partial \phi}{\partial R} = -\frac{4\pi}{\lambda R \tan \theta} B_n \quad (6)$$

Flattening of the interferogram consists of removing the phase component due to the variation of the range distance across the image, i.e.  $\phi_{curved Earth}$ . Removal of this phase term “flattens” the interferogram leaving fringes only related to changes in elevation (as well as noise, atmosphere and surface displacement). The operation is called flattening because in case of a flat surface this would be the only component of the interferometric phase, under the assumption that the other components are null.

Flattening is performed by computation of the fringe rate across the image in order to take into account the variations of slant range distance, incidence angle and perpendicular component of the baseline. This operation assumes the surface of the Earth to be curved (ellipsoid), without topographic features.

## 7. Coherence estimation

Coherence is obtained from the cross-product of the two co-registered SLCs.

Coherence is typically computed as:

$$|\hat{\gamma}| = \frac{\left| \sum_{i=1}^N g_{1,i} g_{2,i}^* e^{-j\phi_i} \right|}{\sqrt{\sum_{i=1}^N |g_{1,i}|^2 \sum_{i=1}^N |g_{2,i}|^2}} \quad (7)$$

where  $e^{-j\phi_i}$  is a correction term related to the local topography. When a DEM is available, it is possible to get to a precise description of the slope correcting factor thus enhancing the accuracy of the coherence estimate. If the DEM is not available, it is possible to derive the correcting factor from the interferogram itself or use an approximation in which the phase is described by either a constant, linear, quadratic or higher order function over the estimation window. The effect of the estimator used on bias and uncertainty of coherence and phase is illustrated in (Dammert, 1996).

The size of the estimation window is a crucial factor determining the coherence estimate. For increasing window size the estimation bias and the estimation uncertainty decrease while the spatial resolution of the coherence image decreases. To compromise between accurate estimation and high spatial resolution, the estimation algorithm can implement adaptive window size depending on an initial estimate of the coherence. In areas of low coherence, larger estimation windows are used (Wegmüller et al., 1998).

Coherence is typically computed using a sliding window. For each pixel the coherence is obtained by applying Equation (7), the window sliding from pixel to pixel. To decrease the effect of resolution loss due to the windowing operation, weighting functions (e.g. linear or Gaussian) can be applied within the window. In this way pixels further away from the centre of the window have less weight on the estimate. The type of weights to be applied depends on the nature of the objects in the scene. If the scene includes distributed targets, weighting plays a minor role. On the contrary, if the scene is populated with small-size point targets, it is recommended to use small windows and strong weighting functions to preserve the coherence of each of the point targets.

Figure 5 illustrates a comparison between two coherence images obtained with different approaches. The images have been acquired on during the ERS-1/2 Tandem mission over Las Vegas, Nevada. The coherence image in Figure 5a has been obtained using a 3x15 window size (3 pixels in range, 15 in azimuth). The coherence image in Figure 5b has been obtained with an adaptive window size varying between 3x15 in high coherence areas and 9x45 in low coherence areas. With an adaptive estimation the contrast has increased since the estimation bias has been reduced, while there has not been any substantial loss in resolution.

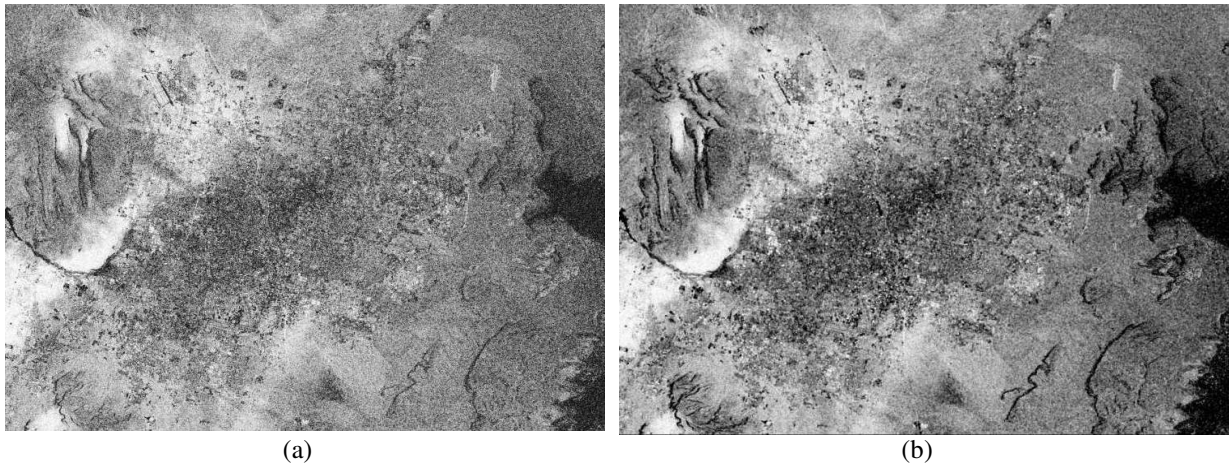


Figure 5. Coherence image from ERS-1/2 Tandem image pair acquired over Las Vegas on 23/24 May 1996 with perpendicular baseline of 106 m. The image is 50 km wide (range direction) and 36 km long (azimuth direction). Processing (a) with a 3x15 large estimation window, (b) with an adaptive estimation method with window size between 3x15 and 9x45 pixels.

## 8. Interferogram filtering

Filtering an interferogram has the objective to reduce phase noise thereby reducing the number of residues. A residue is a point in the interferogram where the sum of the phase differences between pixels around a closed path is not 0.0. Residues exist as pairs. Generally, thermal noise causes pairs of residues that are close together to be generated. The ultimate objective of filtering is to reduce the phase noise and therefore make the phase unwrapping simpler, more robust, and more efficient.

One way of filtering is to multi-look the complex interferogram, i.e. average complex samples. Multi-looking the interferogram reduces the standard deviation of the interferometric phase. The standard deviation of the estimated phase is in fact proportional to the number of pixels over which the average is computed ( $\frac{1}{\sqrt{2N}}$ ). The Cramer-Rao bound for the standard deviation, accurate for  $N > 4$ , is given by:

$$\sigma_{\phi} = \frac{1}{\sqrt{2N}} \frac{\sqrt{1-|\gamma|^2}}{|\gamma|} \quad (8)$$

Other ways of filtering the InSAR phase consist of:

- 2-D band-pass filter the image
- Account adaptively for the local phase gradient.
- Adaptive filtering with filtering function based on local fringe spectrum (Goldstein et al., 1998).

Figure 6 shows a flattened interferogram before filtering and after filtering using the adaptive method based on the local fringe spectrum. While phase noise has been effectively removed, fringes have not been lost.

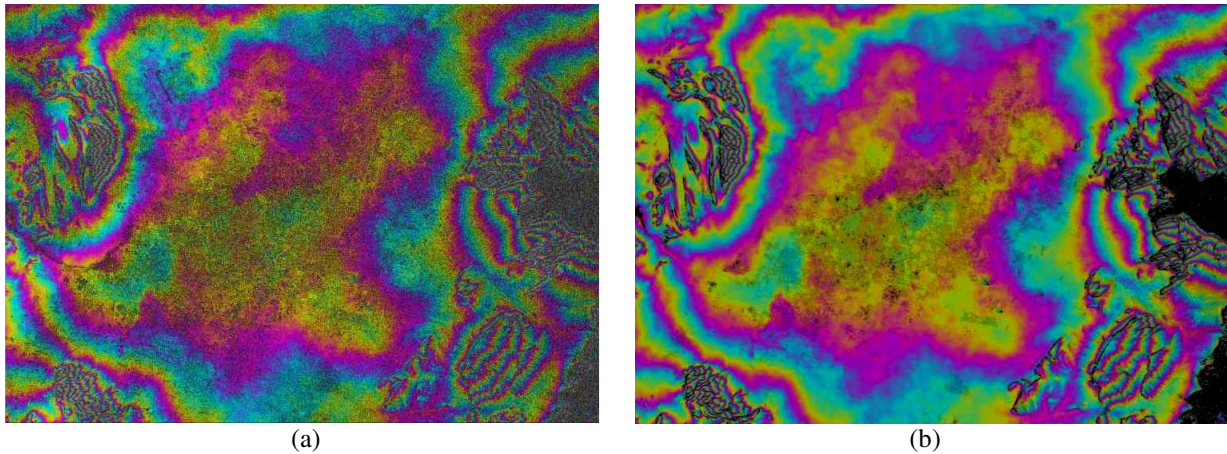


Figure 6. Flattened interferometric phase for the ERS-1/2 Tandem image pair acquired over Las Vegas on 23/24 May 1996 with perpendicular baseline of 106 m, (a) before filtering, (b) filtered with an adaptive filter based on the local fringe spectrum.

## 9. Phase unwrapping

Since the interferometric phase is wrapped modulo  $2\pi$ , an integer number of  $2\pi$  has to be added to recover the absolute phase difference. This operation is called phase unwrapping. Unwrapping the phase means adding a correct multiple of  $2\pi$  to the interferometric phase for each pixel in order to obtain sequential phase values across the entire image.

A fundamental assumption implicit in the phase unwrapping procedure is that the surface is relatively smooth and hence there should be an absence of jumps of the unwrapped phase. More precisely phase unwrapping is based upon the assumption of smooth phase such that the phase differences are  $|\Delta\phi| < \pi$  between adjacent samples. The algorithm must however take into account that actual phase jumps do occur for several reason

- Phase noise: Due to temporal decorrelation, baseline decorrelation, different Doppler centroids, shadow, or low SNR
- Phase undersampling: Steep slopes can cause phase gradients to exceed  $\pi$
- Phase discontinuities: layover and discontinuous surface deformation (earthquake faults, glaciers) lead to phase jumps of multiples of  $2\pi$ .

Figure 7 illustrates a comparison of wrapped and unwrapped phase. Figure 7a shows the unwrapped interferometric phase, where 2 consecutive fringes of the same color have phase difference of  $2\pi$ . Figure 7b shows for the profile indicated by the white line in Figure 7a the wrapped and the corresponding unwrapped phase. While the wrapped phase is between  $-\pi$  and  $\pi$  and shows discontinuities of  $2\pi$  at the extremes of this interval, the unwrapped phase is continuous.

Phase unwrapping is the most crucial step in SAR interferometry, which explain the vast literature published on the subject. A list of relevant publications is provided at the end of this document. Here we introduce two approaches, on which the phase unwrapping methods available in the GAMMA software are based. A more detailed characterization of phase unwrapping solutions, with particular reference to these two methods is provided in (Werner et al., 2002)

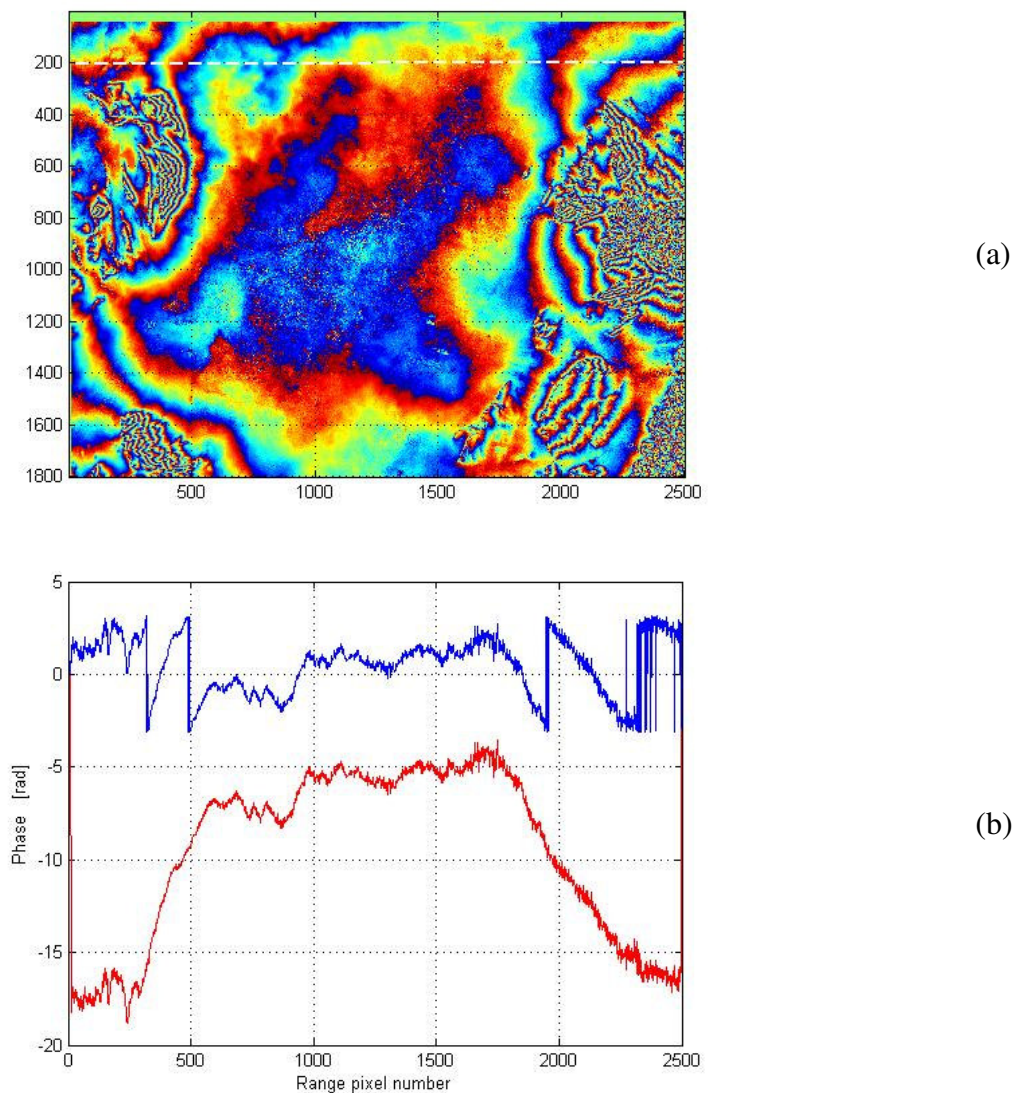


Figure 7. (a) Flattened interferogram as in Figure 7, (b) wrapped (blue line) and unwrapped (red line) phase for the range profile indicated by the white line in the flattened interferogram.

The first method is based on the branch-cut region growing algorithm. This method has been first introduced by REF Goldstein et al., 1988, and detects inconsistencies in the phase data which cause errors in phase unwrapping. These data regions are isolated and only the phase data which give consistent estimates are unwrapped. This algorithm was refined by Rosen et al., 1994, to significantly improve phase unwrapping in regions of high phase noise. In addition, areas of very low degree of coherence are masked to prevent phase unwrapping since the phase values are inaccurate and not useful for estimation of heights or displacements.

The second method uses Minimum Cost Flow (MCF) techniques and a triangular irregular network (TIN). The application of MCF techniques to phase unwrapping and thereby achieve a global optimization was first presented in (Costantini, 1998). The possibility for improving the unwrapping by generalizing the network topology to be a triangulation network was proposed in (Costantini et al., 1999). This technique is a global optimization technique to the

phase unwrapping problem. Other advantages of this technique are that gaps in the input data (for example locations of very low coherence) can be considered and the higher density of the triangular network. Masking, adaptive thinning and patch processing are used to permit efficient and robust unwrapping even of very large interferograms. Compared to the branch-cut region growing algorithm the user interaction is minimal.

## 10. Precise baseline estimation

As mentioned in Section 4, baseline estimation can be performed using several methods. While an initial estimate obtained from orbits or FFT can be considered sufficient to flatten the interferogram, the inversion of the interferometric phase to retrieve elevation requires a more accurate estimate.

To obtain a precise baseline estimate the equation linking topographic phase,  $\phi_{topo}$ , and elevation of a point,  $z$ , can be used:

$$\phi_{topo} = \frac{4\pi B_n}{\lambda R \sin \theta} z \quad (9)$$

where  $\lambda$  represents the wavelength,  $R$  the slant range distance to the point and  $\theta$  the local incidence angle. Knowing height and unwrapped InSAR phase of at least a point on the ground allows getting the baseline

$$B_n = \frac{\lambda R \sin \theta}{4\pi z} \phi_{topo} \quad (10)$$

These ground control points shall be recognizable points in the scene or from a lower resolution DEM co-registered with the unwrapped phase image (i.e. a DEM not in geographical coordinates but transformed into SAR coordinates). There should more points than estimation parameters. It is a good idea to have many more because random errors due to atmosphere, decorrelation, and thermal noise. Sampling over a grid and exclusion of areas of low correlation are recommended. The baseline model takes is a linear function of along-track time or position. A least squares solution for the components is carried out using the unwrapped phase and GCP data. This algorithm finds the set of parameters that minimizes the squared errors. The least squares solution typically converges in 3 to 8 iterations.

This approach is viable if the DEM has sufficient accuracy. The 90m SRTM DEM is a good source for identifying reliable GCPs. In some cases the global DEM GTOPO30 from USGS is adequate for areas with little or moderate terrain variation.

## 11. Computation of heights / resampling to map coordinates

Assuming that the interferometric phase is related to topography only, the inversion of (9) allows obtaining the elevation information from the unwrapped phase. Figure 8 illustrates the elevation obtained from the interferogram of Las Vegas represented in terms of iso-lines. Areas of low correlation have been masked out during phase unwrapping.

The height map obtained at this stage is in radar geometry (slant range / Doppler). For interpretation it is however useful to transform the coordinates from radar geometry to ground range. In this way a rectified height map in orthorectified coordinates following the WGS-84 ellipsoid can be obtained. The rectified height map is in the TCN reference system with the cross-track (C) coordinate following the WGS-84 ellipsoid. The rectification of the height data requires resampling in both azimuth and cross-track directions.

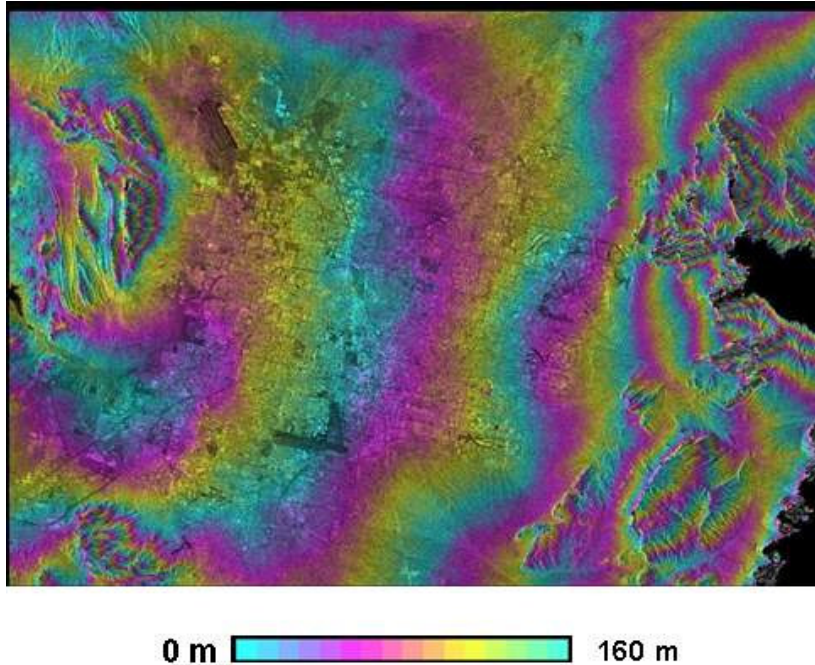


Figure 8. Illustration of elevation retrieved from the unwrapped interferogram of Las Vegas (see Figure 6 for details). In this representation elevation is represented in terms of iso-lines with 160-m spacing between consecutive fringes of the same color.

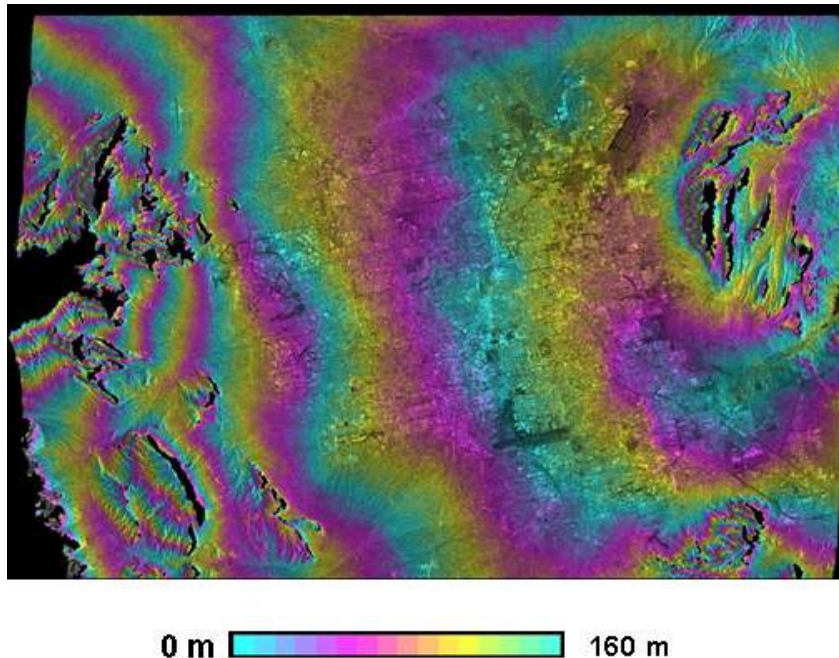


Figure 9. Orthorectified version of the height map of Las Vegas from Figure 8. With respect to Figure 8 the image has also been flipped in order to agree with geographical direction.

Figure 9 illustrates the orthorectified version of the height map shown in Figure 8. Compared to Figure 8 here the image has been flipped horizontally to align the image to the geographical North-South direction and the geographical East-West direction albeit the satellite flying direction.

## **12. Differential interferometric processing**

If the interferometric phase consists of a topographic and displacement term, the processing required to separate these two components goes under the name of differential interferometric processing.

If the aim is to identify the displacement component, the topographic phase has to be removed. This can be determined either from an external DEM from which interferometric fringes are simulated using the parameters of the interferometric system (perpendicular baseline length, slant range distance etc.) or from another interferometric pair, for which one assumes that other phase components are negligible. In this case the fringes have to be scaled to correspond to the perpendicular baseline difference between the differential interferometric pair and the one from which the topography is estimated. When a DEM is available, we speak of 2-pass differential interferometry, otherwise we speak of 3- or 4-pass differential interferometry, this depending on how many images in total are considered to generate the topographic fringes and to obtain the differential interferogram. The following sub-sections describe the processing approaches that allow the separation of the topographic effects from the interferogram to obtain differential phase.

If the aim is to identify the topographic component, the differential phase has to be removed. This can be done by combining complex interferogram and scaling so that phase noise is reduced and an effective baseline larger than the original baselines is obtained. Section 13 describes the processing approach that allows the reduction of the differential interferometric effects to obtain a topographic interferogram.

No matter which component is desired, one should always keep in mind that commonly the interferometric phase has an atmospheric component as well, which induces errors if not accounted for when deriving the height or computing the displacement. If one interferogram is available, the atmospheric phase distortions might severely hinder the correct interpretation of the interferometric phase. It is somehow possible to mitigate the effect of atmospheric phase due to elevation changes using a linear atmospheric model relating the unwrapped phase due to path delays to elevation. If more interferograms are available it is possible to filter them out by stacking the unwrapped phases. While differential signals are correlated, atmospheric phase distortions are random and therefore cancel out when stacking interferograms.

### **12.1. Generation of differential interferogram / removal of topographic phase**

The approaches to obtain a differential interferogram differ depending not only whether a DEM is available or not but also if the phase unwrapping operation is required. Table 1 summarizes the requirement set by each procedure.

Table 1. Approaches of differential interferometry.

Differential interferometric approach	Dataset	DEM	Unwrapping
2-pass differential interferometry	InSAR pair and DEM	External	No
3-pass differential interferometry	3 SAR images (= 2 InSAR pairs)	From one InSAR pair	Yes
4-pass differential interferometry	4 SAR images (= 2 InSAR pairs)	From one InSAR pair	Yes
Combination of complex interferograms	2 InSAR pairs	No	No

The interferogram which contains the differential phase effect (overlaid with the phase due to scene topography) may either be unwrapped before the formation of the differential interferogram or not. The first approach results directly in the unwrapped differential phase. The second approach is a complex differential interferogram which may be filtered and unwrapped after the phase subtraction. Overall phase trends may appear in differential interferograms as a result of inaccurate baseline (respectively orbit) information. Such phase trends may either be removed in the phase subtraction step by using least squares fitting techniques to adjust the scaling of the reference phase image, or, the complex differential interferogram may be flattened using FFT techniques for the estimation of the remaining overall phase trend.

The main advantage of the 3-pass method over the 2-pass method is that no DEM is required. On the other hand the use of a DEM to derive the topographic phase may be used to avoid phase unwrapping problems and to avoid error in the topographic phase due to differential phase effects in the atmosphere and ionosphere.

The main advantage of the 3-pass method over the 4-pass method is that the same reference geometry is used for the two interferograms allowing that an extra registration and resampling step are avoided. On the other hand the use of two completely independent pairs (4-pass method) allows more freedom in the data selection.

#### 12.1.1. 2-pass differential interferometry

The basic idea of 2-pass differential interferometry is that a reference interferogram (interferogram with phase corresponding to surface topography) is simulated based on the DEM. In order to do this the DEM is first transformed from its original coordinate system to the reference SAR image coordinates.

This is done in two steps, which are described more in detail in the DIFF&GEO User's Guide to Geocoding and Image Registration. In a first step the geometric transformation is done based on the available information on the geometry of the DEM and the SAR image geometry used. In the same step the SAR image intensity is simulated based on the simulated local pixel resolution and incidence angle. Inaccurate DEM coordinates, orbit data, and small errors in the calculation of the geometric transformations may result in small offsets between the simulated and the real SAR image geometry. In the second step the offsets between the simulated and real SAR image intensities are estimated and used to accurately register the transformed DEM to the SAR image geometry.

Based on the reference SAR geometry, the interferometric baseline model, and the transformed height map, the unwrapped interferometric phase corresponding exclusively to topography is calculated. In the following this phase will be called topographic phase.

The topographic phase may either be subtracted from the complex interferogram (resulting in a complex differential interferogram) or it may be subtracted from the unwrapped phase (resulting in the unwrapped differential phase). Notice that the complex interferogram does include also the ellipsoidal Earth phase trend, which has to be removed as well.

Generally the available baseline information, especially the one calculated from orbit data, may not be sufficiently accurate thus resulting in a non-perfect compensation for topographic and curved Earth phases. The scaling of the simulated unwrapped phase may be improved by least squares fitting between the simulated and real unwrapped phase image. Notice, that this technique may not work appropriately for ellipsoidal Earth phase trend removed data.

Using 2-pass differential interferometry the generation of a complex differential interferogram is very robust. The generation of the unwrapped differential phase depends on the capability to unwrap either before or after the reference phase subtraction. Especially in terrain with rugged topography the unwrapping of the differential phase (i.e. after the calculation of the phase difference) may be a much easier task than the unwrapping of the phase image which includes both phase due to topography and differential effects.

As an example a geocoded 2-pass differential interferogram for Death Valley is shown in Figure 10. One color cycle corresponds to  $2\pi$  differential phase.

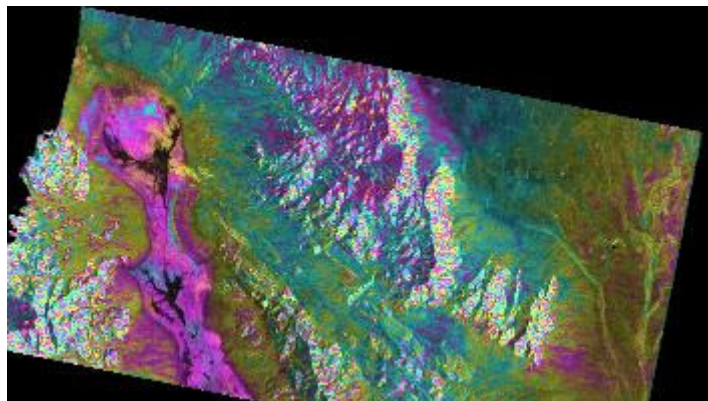


Figure 10. 2-pass differential interferogram of Death Valley.

### 12.1.2. 3-pass differential interferometry

3-pass differential interferometry is based on a SAR image triplet. The geometry of one of the three SAR images is selected as reference geometry. Two interferograms are then generated between the reference pass and the two other passes of the triplet. Selection of identical image sections relative to the reference image ensures that all interferometric products are referenced to the same geometry without extra registration and resampling step.

The idea is that only one of the two interferometric pairs includes differential interferometric phase contributions, while the other one is used as reference to subtract the phase corresponding to the scene topography. Of course, it is not always possible to find ideal triplets for the mapping of a specific displacement event. In addition to data availability problems propagation delay inhomogeneities may occur in the troposphere and ionosphere.

In order to optimize the data selection it has to be kept in mind that the sensitivity of the interferometric phase to topography is proportional to  $1/B_n$  with  $B_n$  the baseline component perpendicular to the line of sight. The sensitivity of the interferometric phase to differential displacement (or phase delays) in the direction of the look vector is independent of the baseline. As a consequence the relative importance of topography and displacement (including propagation delay in homogeneity) depends on the perpendicular component of the baseline. As a reference pair to obtain the phase corresponding to the scene topography a longer baseline is preferred. Yet, it has to be kept in mind that phase unwrapping becomes more difficult with increasing baseline. In order to optimize the sensitivity to differential effects and minimizing the effects of scene topography very short baselines are selected. As additional criteria, the selection needs to take into account that images with high coherence are preferred.

For the 3-pass differential interferometric processing different approaches are used depending on the ability to unwrap the data. There are four possibilities:

Table 2. Approaches of 3-pass differential interferometry.

Case	Interferogram with differential effect	Reference interferogram (to derive phase corresponding to scene topography)
1	Unwrapped phase	Unwrapped phase
2	Unwrapped phase	Complex interferogram
3	Complex interferogram	Unwrapped phase
4	Complex interferogram	Complex interferogram

The complex combination of interferograms allows combining complex interferograms as listed in case 4. Due to the fact that the wrapped phase has to be scaled scaling is restricted to ratios of small integers. The scaling applied can be used to modify the relative importance of topographic and differential phase contributions to the phase of the combined interferogram and has therefore some potential for differential interferometric applications, especially in cases where phase unwrapping failed.

With the GAMMA software cases 1 and 3 can be followed. Since they are based on the unwrapped reference phase, they require successful phase unwrapping of the reference interferogram.

In Case 1 it is assumed that both interferograms, i.e. the interferogram with the differential effects and the reference interferogram used to derive the phase corresponding to scene topography were successfully unwrapped. In the following the phase corresponding to scene topography will also be called topographic phase.

If the ellipsoidal Earth phase trend was removed during the interferometric processing (in order to facilitate filtering, averaging and phase unwrapping) it has to be added back to the unwrapped phase at this point. This step is required to allow the correct scaling of the phases necessary to compensate for the different baselines.

The topographic phase needs to be scaled to account for the different baselines (and corresponding different sensitivities of the interferometric phase to scene topography). The scaling factors may be calculated from the available baseline information. Generally the available baseline information, especially the one calculated from orbit data, may not be sufficiently accurate. Therefore, the scaling of the topographic phase may be improved by

least squares fitting between the topographic phase and the phase of the interferogram which includes the differential effects. Notice, that this technique may not work appropriately for ellipsoidal Earth phase trend removed data. After determination of the scaling factors with the least squares approach the scaled topographic phase is subtracted from the unwrapped phase. The phase difference image corresponds to the unwrapped differential phase.

In Case 3 it is assumed that the unwrapped phase is available only for the reference interferograms, i.e. the interferogram used to derive the phase corresponding to scene topography. If the ellipsoidal Earth phase trend was removed during the interferometric processing (in order to facilitate filtering, averaging and phase unwrapping) it has to be added back at this point. This use of the original phase is required for the correct scaling of the phases necessary to compensate for the different baselines.

The topographic phase needs to be scaled to account for the different baselines (and corresponding different sensitivities of the interferometric phase to scene topography). The scaling factors are calculated from the available baseline information. Generally the available baseline information, especially the one calculated from orbit data, may not be sufficiently accurate. As a result the complex differential interferogram obtained after subtraction of the scaled topographic phase may still show an overall phase trend. This overall phase trend may be retrieved using a 2-D FFT and then removed.

The method described as Case 3 is slightly more robust than the one described in Case 1 because phase unwrapping is required only for the reference interferogram. As an example a 3-pass differential interferogram for Death Valley (in SAR geometry) is shown below. One color cycle corresponds to 2PI differential phase.

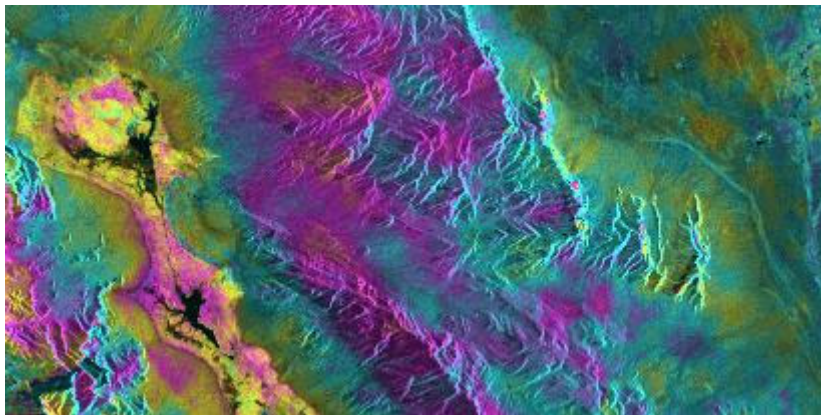


Figure 11. 3-pass differential interferogram of Death Valley.

### 12.1.3. 4- pass differential interferometry

The 4-pass method is very similar to the 3-pass method with the exception that different reference geometries are used for the interferometric processing of the two interferograms (no common pass). As a consequence, the interferometric products of the reference interferogram (defined as the interferogram used to derive the phase corresponding to scene topography) need to be transformed into the reference geometry of the other interferogram (i.e. the interferogram which includes the differential effects).

The idea is that only one of the two interferometric pairs includes differential interferometric phase contributions, while the other one is used as reference to subtract the phase

corresponding to the scene topography. Of course, it is not always possible to find ideal quadruplets for the mapping of a specific displacement event. In addition to data availability problems, propagation delay inhomogeneities may occur in the troposphere and ionosphere.

In order to optimize the data selection it has to be kept in mind that the sensitivity of the interferometric phase to topography is proportional to  $1/B_n$  with  $B_n$  the baseline component perpendicular to the line of sight. The sensitivity of the interferometric phase to differential displacement (or phase delays) in the direction of the look vector is independent of the baseline. As a consequence the relative importance of topography and displacement (including propagation delay inhomogeneity) depend on the interferometric baseline (component perpendicular to look vector). As a reference pair to obtain the phase corresponding to the scene topography a longer baseline is preferred. Yet, it has to be kept in mind that phase unwrapping becomes more difficult with increasing baseline. In order to optimize the sensitivity to differential effects and minimizing the effects of scene topography very short baselines are selected. As an additional criterion the selection needs to take into account that images with high coherence are preferred.

The geometric transformation of the reference interferogram into the geometry of the other interferogram consists basically of two steps. In the first step the registration offset polynomials (describing the range and azimuth offsets between the geometries of the two interferograms as linear functions of range and azimuth) are determined. This is done by an initial offset estimation followed by the accurate estimation of the offset polynomials. Both, initial and precision estimation are based on the SAR image intensities. Complex cross-correlation registration approaches might only be applied in cases with sufficiently high coherence between the two data sets. This restriction does not apply to the registration approach based on the image intensity, which has therefore a wider range of applicability and higher robustness. Once the registration function is known both real and complex valued data sets can be resampled to the reference geometry.

After transforming the unwrapped phase and/or the complex interferogram of the reference pair the same approaches as for the 3-pass interferometry can be followed. Different approaches are used depending on the ability to unwrap the data. There are the same four cases as described in the section on the 3-pass method. For a discussion of the formation of the complex differential interferogram, and the differential phase image it is referred to the section on the 3-pass differential interferometry.

#### 12.1.4. Combination of interferograms

The "wrapped" interferometric phase, i.e. the phase information available from an interferogram without phase unwrapping, is defined as the "unwrapped" interferometric phase modulo  $2\pi$

$$\phi_{unw} \bmod 2\pi = \phi$$

When scaling the interferometric phase, which is of interest for example to simulate the interferogram obtained with another baseline, we have to be aware of the fact that in principle the "unwrapped" interferometric phase needs to be scaled. When scaling with a positive or negative integer number the scaling of the "wrapped" phase may be directly scaled as the unknown number  $i$  of  $2\pi$  remains an integer even after the scaling, i.e.

$$\left( x\phi_{unw} \right) \bmod 2\pi = x\phi + (x \cdot i \cdot 2\pi) \bmod 2\pi \begin{cases} = x\phi & x \in \text{integers} \\ \neq x\phi & x \notin \text{integers} \end{cases}$$

The combination of complex interferograms after scaling of the "wrapped" interferometric phase with integer numbers may be of interest to do a kind of differential interferometry without phase unwrapping and geocoding requirement.

The sensitivity to the topography is reduced as much as possible, in order to have a phase of the combined complex interferogram which is mainly determined by differential effects. The reduction of the sensitivity to topography is achieved by reducing the "simulated" baseline of the combined interferogram to a small value. A perpendicular baseline component of the combined interferogram of only 10m, for example, can be achieved by combination of two interferograms with perpendicular baseline components of 50m and 160m through scaling of the wrapped phases with factors of 3 and -1, respectively. In this example the unwrapped phase of the combined interferogram corresponds to the topographic phase of an interferogram with a 10 m baseline (i.e. a very small sensitivity to topography), plus 3 times the differential phase effects present in the first interferogram minus 1 time the differential phase of effects present in the second interferogram.

## 12.2. Extraction of topographic phase / removal of differential phase

Combination of interferograms can also be used to improve the sensitivity to topography. With this method the phase noise and the sensitivity to differential effects are reduced and the sensitivity to topography is increased. The reduction of the sensitivity to differential effects is achieved simply by addition of independent interferograms. Assuming that the unwanted differential effects (mainly atmospheric distortions) of the two interferograms are independent, the combination of interferograms allows decreasing their influence. At the same time the baseline of the combined interferogram may be increased as compared to the initial interferograms. Because the phase noise of the individual interferograms is multiplied with the scaling factors small scaling factors are preferred. The combination of two independent interferograms with comparable perpendicular baseline components (using scaling factors of 1), for example, increases the simulated baseline of the combined interferogram to twice that of the individual interferograms with a phase noise of the combined interferogram of only about 1.4 times that of the individual interferogram.

About the same technique but for another purpose was presented by Massonnet et al., 1996. Their idea was to generate combined interferograms with relatively small baselines in order to reduce the need of phase unwrapping.

As an example of an interferogram with a "combined" perpendicular baseline component of 21m obtained by combining registered complex interferograms of 58m and 95m perpendicular baseline components using phase scale factors of 2 and -1, respectively, for Solothurn, Switzerland.

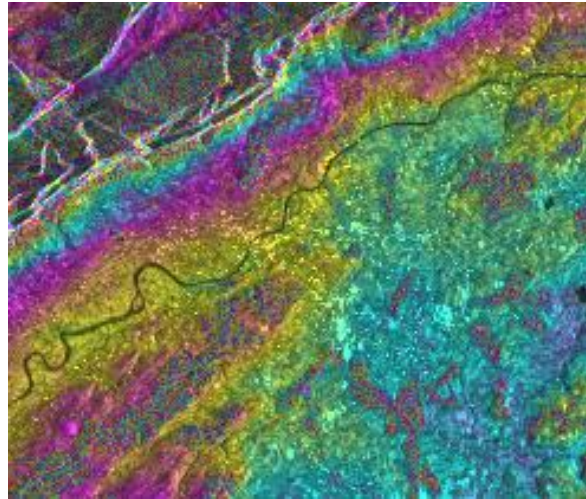


*Figure 4. Combined interferogram based on two ERS tandem interferograms with perpendicular baseline of 58 m and 95 m respectively. The resulting interferogram has 21 m perpendicular baseline.*

## References

- Costantini, M., "A novel phase unwrapping method based on network programming," *IEEE Transactions on Geoscience and Remote Sensing*, vol. 36, 3, pp. 813-821, 1998.
- Costantini, M., Rosen, P. A., "A generalized phase unwrapping approach for sparse data," *Proceedings of IGARSS'99*, Hamburg, 28 June-2 July, pp. 267-269, 1999.
- Dammert, P. B. G., "Accuracy of INSAR measurements in forested areas," *Proceedings of 'Fringe 96' Workshop on ERS SAR Interferometry*, Zürich, 30 September - 2 October, pp. 37-49, 1996.
- Gatelli, F., Monti Guarnieri, A., Parizzi, F., Pasquali, P., Prati, C., Rocca, F., "The wavenumber shift in SAR interferometry," *IEEE Transactions on Geoscience and Remote Sensing*, vol. 32, 4, pp. 855-865, 1994.
- Goldstein, R. M., Zebker, H. A., Werner, C. L., "Satellite radar interferometry: Two-dimensional phase unwrapping," *Radio Science*, vol. 23, 4, pp. 713-720, 1988.
- Goldstein, R. M., Werner, C. L., "Radar interferogram filtering for geophysical applications," *Geophysical Research Letters*, vol. 25, 21, pp. 4035-4038, 1998.
- Massonnet D., Vadon, H., Rossi, M., "Reduction of the need for phase unwrapping in radar interferometry," *IEEE Transactions on Geoscience and Remote Sensing*, vol.34, 2, pp.489-497, 1996.
- Rosen, P. A., Werner, C. W., Hiramatsu, A., "Two-dimensional phase unwrapping of SAR interferograms by charge connection through neutral trees," *Proceedings of IGARSS'94*, Pasadena, 8-12 August, 1994.
- Schwäbisch, M., Geudtner, D., "Improvement of phase and coherence map using azimuth prefiltering: Examples from ERS-1 and X-SAR," *Proceedings of IGARSS'95*, Florence, 10-14 July, pp. 205-207, 1995.
- Touzi, R., Lopes, A., Bruniquel, J., Vachon, P. W., "Coherence estimation for SAR imagery," *IEEE Transactions on Geoscience and Remote Sensing*, vol. 37, 1, pp. 135-149, 1999.
- Wegmüller, U., Werner, C., Strozzi, T., "SAR interferometric and differential interferometric processing," *Proceedings of IGARSS'98*, Seattle, 6-10 July, pp. 1106-1108, 1998.
- Werner, C., Wegmüller, U., Strozzi, T., Wiesmann, A., "Processing strategies for phase unwrapping for INSAR applications," *Proceedings of European Conference on Synthetic Aperture Radar EUSAR 2002*, Cologne, 4-6 June, pp. 353-356, 2002.

## **Additional bibliography on SAR interferometric processing**

- Bamler, R., Hartl, P., "Synthetic aperture radar interferometry," *Inverse Problems*, vol. 14, 4, pp. R1-R54, 1998.
- Bürgmann, R., Rosen, P. A., Fielding, E. J., "Synthetic aperture radar interferometry to measure Earth's surface topography and its deformation," *Annual Review of Earth and Planetary Science*, vol. 28, pp. 169-209, 2000.
- Gens, R., van Genderen, J. L., "Review Article: SAR interferometry - issues, techniques, applications," *International Journal of Remote Sensing*, vol. 17, 10, pp. 1803-1835, 1996.
- Gens, R., "The influence of input parameters on SAR interferometric processing and its implication on the calibration of SAR interferometric data," *International Journal of Remote Sensing*, vol. 21, 8, pp. 1761-1771, 2000.
- Goldstein, R. M., Zebker, H. A., Werner, C. L., "Satellite radar interferometry: Two-dimensional phase unwrapping," *Radio Science*, vol. 23, 4, pp. 713-720, 1988.
- Graham, L. C., "Synthetic interferometer radar for topographic mapping," *Proceedings of the IEEE*, vol. 62, 6, pp. 763-768, 1974.
- Just, D., Bamler, R., "Phase statistics of interferograms with applications to synthetic aperture radar," *Applied Optics*, vol. 33, 20, pp. 4361-4368, 1994.
- Madsen, S. N., Zebker, H. A., "Imaging Radar Interferometry," in *Principles and Applications of Imaging Radar*, vol. 2, *Manual of Remote Sensing*, Henderson, F. M., and Lewis, A. J., Eds., 3rd ed. New York: John Wiley & Sons, pp. 359-380, 1998.
- Massonnet, D., Feigl, K. L., "Radar interferometry and its application to changes in the Earth's surface," *Reviews of Geophysics*, vol. 36, 4, pp. 441-500, 1998.
- Rosen, P. A., Hensley, S., Joughin, I. R., Li, F. K., Madsen, S. N., Rodriguez, E., Goldstein, R. M., "Synthetic Aperture Radar Interferometry," *Proceedings of the IEEE*, vol. 88, 3, pp. 333-382, 2000.
- Sandwell, D. T., Price, E. J., "Phase gradient approach to stacking interferograms," *Journal of Geophysical Research*, vol. 103, B12, pp. 30,183-30,204, 1998.